Developments in the Built Environment 20 (2024) 100558

Contents lists available at ScienceDirect

Developments in the Built Environment

journal homepage: www.sciencedirect.com/journal/developments-in-the-built-environment

Grain-size composition effect on flexural response and pore structure of cementitious tail-rock fills with fiber reinforcement

Hao Qin [a,b], Shuai Cao [a,b,**], Erol Yilmaz [c,*]

[a] State Key Laboratory of High-Efficient Mining and Safety of Metal Mines of Ministry of Education, University of Science and Technology Beijing, Beijing, 100083, China
[b] School of Civil and Resource Engineering, University of Science and Technology Beijing, Beijing, 100083, China
[c] Department of Civil Engineering, Geotechnical Division, Recep Tayyip Erdogan University, Fener, Rize, TR53100, Türkiye

ARTICLE INFO

Keywords:
Cementitious tail-rock fill
Gravel rock
Grain size
Fiber reinforcement
Flexural features

ABSTRACT

This paper explores the grain-size composition effect on flexural and micro-structural features of fiber reinforced cementitious tail-rock fill (FRCTRF). The FRCTRF mixes considered contained a stationary solid concentration of 70 wt% and a cement/tail rate of 1:6, and were cured for an age of 7-day for strength tests and microstructure. Three-point bending test shows that FRCTRF's bending property is upgraded by totaling gravel rock. Adding fiber to FRCTRF's bottom can enhance its peak deflection. With rising gravel particle size/dosage, FRCTRF's peak deflection displays a trend of falling first and then growing. Accumulating polypropylene fiber could advance FRCTRF's post-peak strength features as well. FRCTRF sample containing gravel has a large stress drop, and adding gravel rock could essentially boost FRCTRF's post-peak brittle-ability. In conclusion, this study provides a strong scientific and theoretical underpinning for optimizing artificial false roofs employed recently in modern underground metalliferous mining operations.

1. Introduction

Ore deposits enclosing valuable minerals are important ways to safeguard the national economy (Xue et al., 2023). While mining brings huge profits, it also creates natural destructions like surface subsidence (Wang et al., 2023a), aquifer structures' devastation (Wang et al., 2023b), and large waste production (specially gravel rock and tailings (Yang et al., 2024)). Realizing the resource use of tailings, gravel rock, and other wastes is an important way for green development (Li et al., 2021; Sadrossadat et al., 2020; Yilmaz et al., 2013). Tailings and gravel rock are made into fill ingredients, which alleviate the tricky of surface subsidence and dispose of mine waste (Qi and Fourie, 2019). Mining filling system is booming, the downcut backfill mining system can prevent workers from working under the exposed roof, and in mining process using downcut filling technique, construction of a strong artificial roof is very critical (Yan et al., 2022). The consolidated fill technology includes cemented tailings fill/cemented paste fill (CTF/CPF (Yang et al., 2023; Yilmaz et al., 2010; Carnogursky et al., 2023),). Traditional fill materials are customarily made by blending tail/cement/water (Yu et al., 2022). Curing conditions (i.e., time (Sari et al., 2023), temperature (Bull and Fall 2020)), experimental tool (Benzaazoua et al., 2006), aggregate grading (Lyu et al., 2023), chemical composition (Koohestani et al., 2018), and cement type (Perumal et al., 2020) tend to affect traditional fill's strength features (Jiang et al., 2024a). The greater the proportion of a given binding type in CTF/CPF, the better the mechanical properties (Zhang et al., 2022; Johansson et al., 2024). Nevertheless, even a slight escalation in the cement dosage will unavoidably upsurge the costs of mining and backfilling operations, negatively affecting sustainable growth in mines (Fang et al., 2023).

Some researchers (Hu et al., 2024; Kasap et al., 2022; Jiang et al., 2024b; Zhu et al., 2024a) have exposed that totaling certain additives to the fill mixtures could boost their strength features. To end up this research gap, scholars have fulfilled large quantities of works on enhancing strength features of the backfill with various additives, covering fibers (i.e., polypropylene (Hou et al., 2023), polyacrylonitrile (Huang et al., 2021), glass (Jan et al., 2022), polyvinyl alcohol (Li et al., 2023a), basalt (Wang et al., 2023c), and palm (Chompoorat et al., 2023)) and others (i.e., Alfa (Ajouguim et al., 2023), straw (Chen et al., 2020), jute (Jo et al., 2015), metakaolin (Niu et al., 2020), and rubber (Wang et al., 2021a)). Advancing 3D printing technology (Bianchi et al.,

* Corresponding author.
** Corresponding author. State Key Laboratory of High-Efficient Mining and Safety of Metal Mines of Ministry of Education, University of Science and Technology Beijing, Beijing, 100083, China.
E-mail addresses: qh32001@163.com (H. Qin), sandy_cao@ustb.edu.cn (S. Cao), erol.yilmaz@erdogan.edu.tr (E. Yilmaz).

https://doi.org/10.1016/j.dibe.2024.100558
Received 1 August 2024; Received in revised form 8 September 2024; Accepted 10 October 2024
Available online 18 October 2024
2666-1659/

Fig. 1. Particle diameter gradations of gravel rocks: (a) 1–2 mm; (b) 2–4 mm; (c) 4–6 mm.

2024; Dong et al., 2022; de Moraes et al., 2024) has recently appealed attention for those doing research in civil and mining engineering fields. Hence, some researchers (Samiratou Yaya et al., 2024; Gencel et al., 2022; Zhao et al., 2023a) have used 3D printing technology to produce 3D printing polymer mesh to enhance fill's mechanical properties. Some other enhancement additives such as carbon nanotubes, nanocellulose, and cellulose acetate have also attracted scholars' attention, and these additives have good modification properties (Falliano et al., 2022; Zou et al., 2024; Qiu et al., 2023). Compared with non-fiber-reinforced CTF, composite fiber-reinforced CTF has been determined to enhance mechanical properties (Zhang et al., 2023). Some scholars (Zhu et al., 2024b; Haruna and Fall 2022) have explored the suitability of filling underground gobs enriched with cement-based constituents and fiber reinforcement. Researchers have studied tensile features (Dash et al., 2023), freeze-thaw features (Jiang et al., 2017), dynamic load properties (Qin et al., 2021), microscopic composition (Zhang et al., 2024), temperature influence rule (Xu et al., 2022), and durability (Guler and Akbulut, 2023) of fiber reinforced cementitious materials (Zou et al., 2023) based on influencing factors such as fiber length (Hou et al., 2024), type (Xu et al., 2019) and content (Consoli et al., 2017). Sun et al. (2023) used scanning electron microscope (SEM) and Particle Flow Code 3D (PFC 3D) model to further study failure approach and fiber strengthening mechanism of layered CTF (LCTF) with fiber reinforcement. Jiang et al. (2022) modified composite fiber two-ash by uniaxial-compressive and splitting-tensile experiments. Mechanical properties of iron tailings were analyzed while acquiring the optimum ratio of LCTF specimens. Xue et al. (2021) scrutinized impact of type/-content of fiber, solid dosage, and binder-tail (b/t) rate on CTF's crack/post peak toughness through orthogonal design scheme's three-point bending experiment. Wang et al. (2024) studied strength features of CTWRB subjected to diverse proportions, and analyzed influence of aggregate PSD under continuous gradation on strength properties of CTWRB. Komurlu (2023) used micro-grid fiber as an innovative stabilizer to further enhance cement-based rock fills' compressive/tensile strengths. Naoum et al. (2023) assessed the capacity of PZT-based SHM method for identifying changes in structural integrity of a RC structure by connecting PZT sensors having numerous arrangements. Ahmad et al. (2021) studied the features of fibers and their inducing factors on FRCBM's damaging characteristics.

Mining waste restricts its development prominently (Xu et al., 2020; Li et al., 2023b). In particular, the crushed stone left in the mining process is employed to partly substitute tailings to formulate crushed stone-tails consolidated backfill into the goaf, and its mechanical characteristics attract the research of researchers. Huang et al. (2023) used uniaxial compressive strength (UCS) experiment and SEM micrographs to further investigate microstructure/strength performance of gellable tailor-rock crushing fill containing gold/tungsten tails and rocks. Qin et al. (2024) studied impacts of grain-size composition on strength, energy and structural features of cement-based tail-rock fill (CTRF) containing a solid fraction of 70 wt%. Qiu et al. (2022) tested acoustic emission features of tail-waste rock fill subjected to uniaxial compression conditions and obtained fill's strength and deformation characteristics. Zhao et al. (2023b) established a new CTRF strength development model having waste rock mass fraction and damage coefficient defined as key factors. Yin et al. (2023) inspected experimentally the strength characteristics of cementitious tailings waste fill (CTWF) by combining extensive laboratory testing with deep learning. Gao et al. (2023) set diverse amounts of waste rocks and tails and solidification heats to investigate impact of diverse circumstances on cemented fill's porosity/strength property. In addition, mine-fill engineering is affected by practical factors and often adopts the method of stratified fill, so artificial stratified interface deserves attention (Wang et al., 2021b). Jiao et al. (2023) scrutinized the impacting mechanism of boundary irregularity on bonding quality of layered cementitious fills by using UCS experiment, and surface roughness/particle size detection. Li et al. (2023c) quantitatively analyzed LCTF's porosity and density in the course of the solidity (compression) process through expending gray-scale parameters of X-ray computed tomography scan pictures.

At present, strength features, failure approaches, and microstructure of fills with fiber reinforcement and solid waste modified fills were studied under different test conditions. However, due to rock fragment content/particles, laboratory studies of strength/microstructure features of fiber reinforced cementitious tail-rock fill (FRCTRF) samples are still strictly required. This paper innovatively leads new rehearsal of joining crushing stone into FRCTRF's upper layer. To study strength impact and mechanism of composite FRCTRF samples, SEM micromorphology and EDS analysis were observed while three-point tensile experiment was undertaken in well-equipped lab environment. Diverse classes of FRCTRFs were created by bearing in mind diverse gravel dosage and grain dimeter.

2. Materials and methods

2.1. Materials

2.1.1. Gravel rock

Gravel rock (contains no clay and limited fine particles or dust) comes from a Chinese mine, and is employed to make filling specimens. Porosity, water content and specific gravity of rock is 47.6 %, 8.93 %, and 1.72, respectively. Particle dimeter gradations of the rocks are divided into three groups: 1–2 mm, 2–4 mm, 4–6 mm (Fig. 1). Maximum particle diameter of rock (20 mm) does not exceed one-fifth of mold's interior particle. Rock particles are graded by the matching displacement method, and the weighted mean value of rock particles with a particle of 5–20 mm is used to replace the content of large rocks.

2.1.2. Mineral tailings and binders

The coarse-sized tails covering active components provided by a

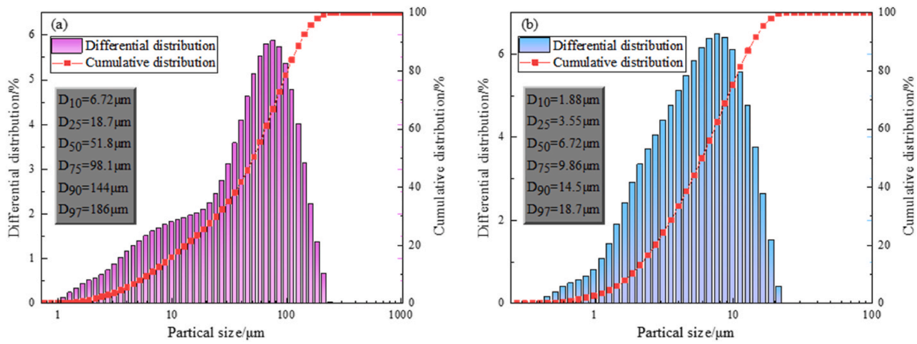

Fig. 2. Grain sizes and profiles of tailing (a) and binding (b).

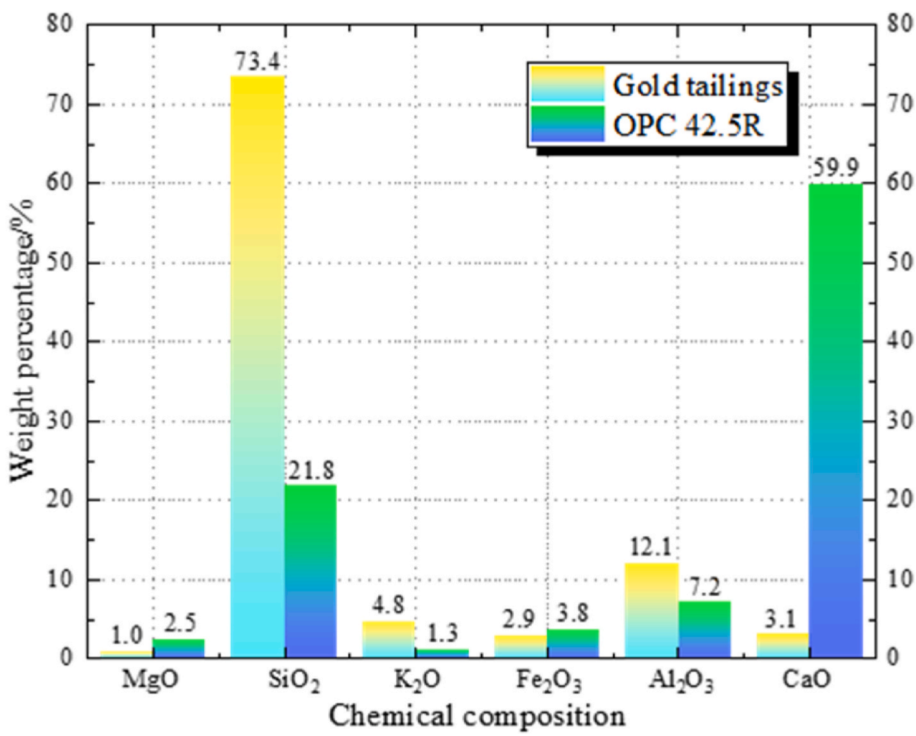

Fig. 3. Oxide configuration of tailing and binding specimens.

metallic U/G mine in Shandong were employed as the key solids in the lab test. OPC (normal Portland binder class 42.5 R) is nominated as a fundamental cement for the formation of fill bodies. Tail's/binder's particle widths and distributions was distinguished using a Rigaku Ultima IV X-ray diffractometer (XRD) tool. Fraction of smaller particles (less than 20 μm) affecting FRCTRF's rigidity, flow, and microstructure was 49.8 wt% (Fig. 2). Note that ordinate in Fig. 2 is the volume fraction.

Tails'/binder's oxide analyses were detected via a scanning XRF-1800 (Fig. 3). Test parameters are: skimming rapidity 300 s/min, power 60 kV, current 140 mA. One can observe that tails'/cement's CaO content is the highest, which is 56.4 % and 52.2 % respectively.

2.1.3. Fiber

According to earlier studies, adding polypropylene fiber (PP fiber) to CTF can increase its deflection/flexural strength (FS). In this study, only PP fiber reinforced FRCTRF was used. Being an efficient reinforcement product, PP has a better elasticity and ductility than others. The length, density, tensile strength, and elongation parameters of PP fiber are respectively 12 mm, 0.89 g/cm^3, 398 MPa, and 28 %.

2.2. Forming and curative practices

The current work's basic intention is to study impact of gravel rock dosage/particle size on FRCTRF's strength characteristics. The gravel content in FRCTRF was taken into account as a control group (0 % control), and 3 diverse gradations: 10 %, 30 %, and 50 %. 3 diverse grades of 1–2 mm, 2–4 mm, and 4–6 mm were employed to create FRCTRF specimens. They were cast into layers holding a height of 20 mm. In this study, part of the crushed stone was used to replace the mortar pouring of tailings in the upper layer, and the mortar with PP fiber was used to pour in the lower layer. According to the previous research, CTF performance was the best as the rate of PP fiber was 0.6 %, so lower mortar's fiber dosage was 0.6 %. The mortar covers cement/tail (c/t) rate of 1:6 so that solid concentration of FRCTRF sample is 70 wt% and subjected to curing at a constant period of 7-day. The prepared fills were poured into a cuboid mold holding length × width × height: 160 × 40 × 40 mm. To obtain accurate laboratory strength numbers, mean strengths after experiments is taken by removing unusual strength numbers.

Prior to fill preparations, layer height was marked on the entire molds with a pencil. Usual automatic scales are employed to accurately

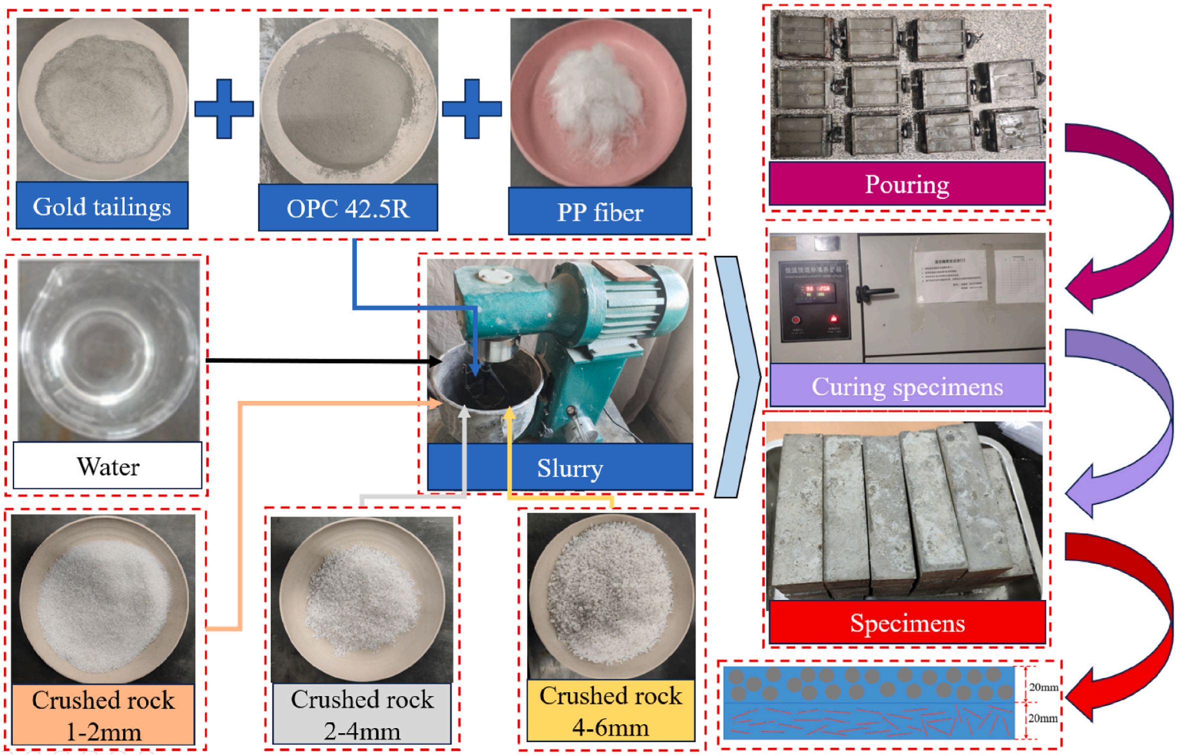

Fig. 4. FRCTRF's creating practices in a well-equipped lab environment.

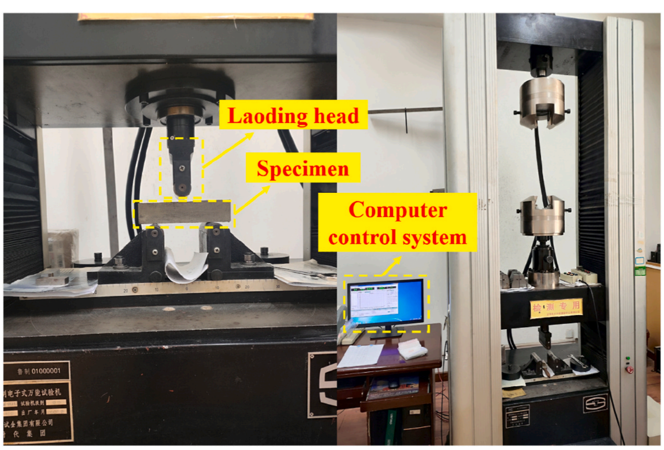

Fig. 5. A laboratory tool for detecting FRCTRF's flexural strengths.

detect masses of tails/cement/water. Following completing those stages, all elements were cast in a blender and mix methodically for 190 s. During the mixing process, a pre-determined volume of water is appended and blend continues for 3 min. Then, all the prepared filling slurry was put in all specimens' bottom layer and left for 60 min 1-h later, the upper filling slurry was created by reiterating the whole process, and each mold was poured. FRCTRF specimens are stored in a small container holding fixed heat (20 ± 1 °C) and wetness (98 ± 2 %). The separate demolding time of the entire fills was 2-day. Fig. 4 shows FRCTRF's creating ways being applied in the current trial.

2.3. Three-point bending test

After the corresponding curing age (7 day), the bending/flexural performance of the FRCTRF is tested by 3-point bending. The strength trial was fulfilled by a fully automatic testing tool (model WDW-200 D, max. load:200 kN). The backing point span and pressure speed are 100 mm and 0.5 mm/min, respectively. Computer can record all the tests automatically. At the same time, CTF specimens were photographed with cameras for subsequent analysis. In this study, at least 3 specimens of each formulation mix were verified for reading strengths, and mean result is accepted as ultimate flexural strength. Fig. 5 demonstrates experiment tool being applied in the current work.

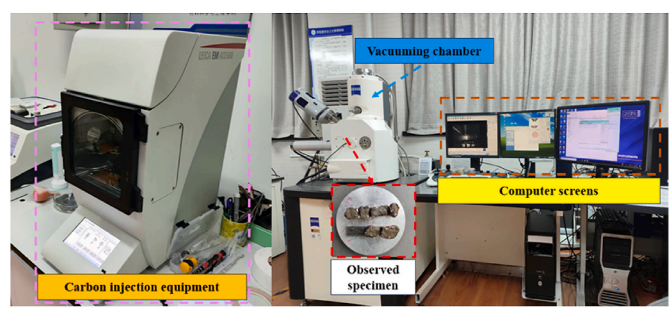

Fig. 6. A laboratory tool for interpreting FRCTRF's microstructures.

2.4. SEM-EDS clarifications

To detect FRCTRF's morphology/microstructure, an advanced tool called Zeiss EVO18 (SEM-EDS) has been employed (Fig. 6). This advanced system is implemented by using LaB6/W filament for image measurement and analysis. During SEM observation, the test limit is an extreme accelerating voltage of 20 kV and a tenacity of 3 nm. During energy dispersive spectrometry test (EDS), the limits considered were: high voltage 15 kV, image size 1000 × 750. Before SEM, the filled sample was first dehydrated and then carbon-sprayed twice with the LEICA EM ACE600 device. FRCTRF sample to be experienced is placed in a space chamber where air is completely emptied.

Table 1
FRCTRF recipes.

Sample ID	FS[a] (MPa)	SD[b]	COV[c]	Specimen ID	FS[a] (MPa)	SD[b]	COV[c]	Specimen ID	FS[a] (MPa)	SD[b]	COV[c]
10%-1-2-1	0.93	0.0449	0.0481	30%-1-2-1	0.87	0.0362	0.0395	50%-1-2-1	0.92	0.0216	0.0239
10%-1-2-2	0.98			30%-1-2-2	0.94			50%-1-2-2	0.90		
10%-1-2-3	0.89			30%-1-2-3	0.93			50%-1-2-3	0.88		
Average:	0.93			Average:	0.92			Average:	0.90		
10%-2-4-1	1.02	0.0639	0.0622	30%-2-4-1	1.00	0.1195	0.1284	50%-2-4-1	1.00	0.0751	0.0797
10%-2-4-2	0.96			30%-2-4-2	0.79			50%-2-4-2	0.97		
10%-2-4-3	1.09			30%-2-4-3	1.00			50%-2-4-3	0.86		
Average:	1.03			Average:	0.93			Average:	0.94		
10%-4-6-1	1.19	0.0633	0.0556	30%-4-6-1	1.05	0.1144	0.1217	50%-4-6-1	0.99	0.0520	0.0529
10%-4-6-2	1.07			30%-4-6-2	0.83			50%-4-6-2	1.02		
10%-4-6-3	1.16			30%-4-6-3	0.94			50%-4-6-3	0.95		
Average:	1.14			Average:	0.94			Average:	0.98		
0%-1-1	0.70	0.0373	0.0704	0%-2-1	0.76	0.0521	0.0494				
0%-1-2	0.77			0%-2-2	0.79						
0%-1-3	0.74			0%-2-3	0.72						
Average:	0.74			Average:	0.76						

[a] FS stands for flexural strength.
[b] SD: Standard deviation.
[c] COV: Coefficient of variation.

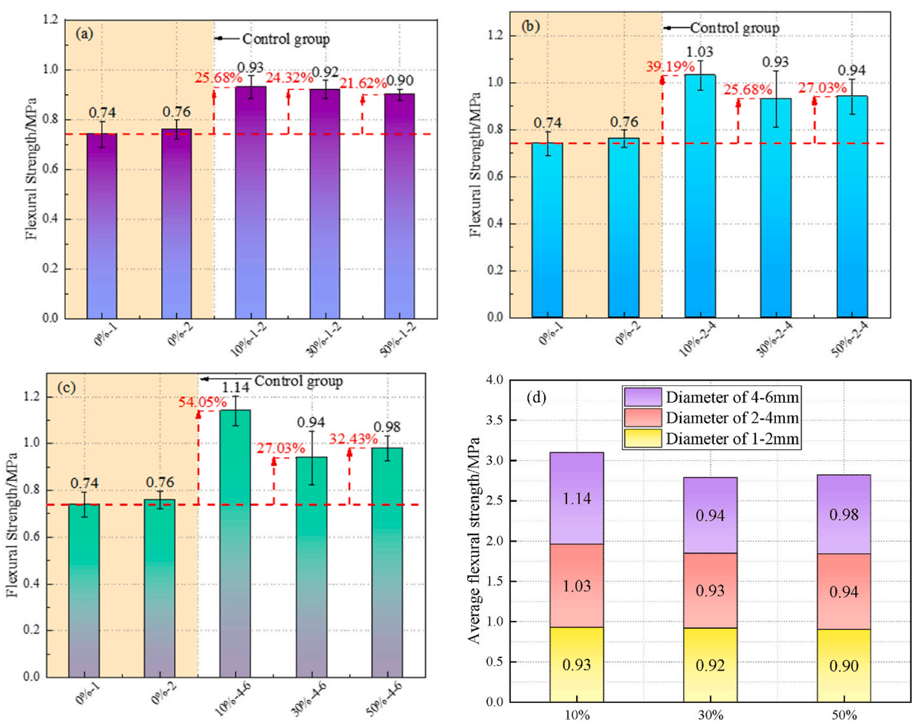

Fig. 7. Gravel rock rate influence on mean Flexural Strength behavior of FRCTRFs: (a) particle of 1–2 mm; (b) particle of 2–4 mm; (c) particle of 4–6 mm and (d) Stacking diagram under the influence of content.

3. Results and discussion

3.1. Assessing flexural strength of FRCTRF

Accompanied by the requirements of three-point flexural tests, a formulation detecting the flexural strength of FRCTRF is given below (Xue et al., 2022):

$$\sigma = \frac{3PL}{2bh^2} \tag{1}$$

where P is peak stress; L is distance amid upper/lower plates; b is layer width; h is layer height.

Table 1 shows the flexural strength under different particles and gravel rocks. For convenient description, the sample is named in the way of "content - particle size - number". Two control groups were set up, where "0%-1-1", "0%-1-2" and "0%-1-3" were sample without gravel rock and fiber, and "0%-2-1", "0%-2-2", and "0%-2-3" were sample without gravel rock but with fiber in the lower layer. And "0%-2" was sample without gravel rock but with fiber in the lower layer (total number of prepared samples 30). "0%-2" was sample without gravel rock but with fiber in the lower layer. "1–2", "2–4", and "4–6" represent specimens with 1–2 mm, 2–4 mm, and 4–6 mm gravel added, respectively. Take the number "10%-1-2" as an instance, "10%" and "1–2" signify 10% rock dosage and 1–2 mm rock grain diameter. In the table, "1, 2 and 3" signify the sum of parallel samples. Table 1 shows the average flexural strength, standard deviation, and coefficient of variation of each specimen after 7-day curing.

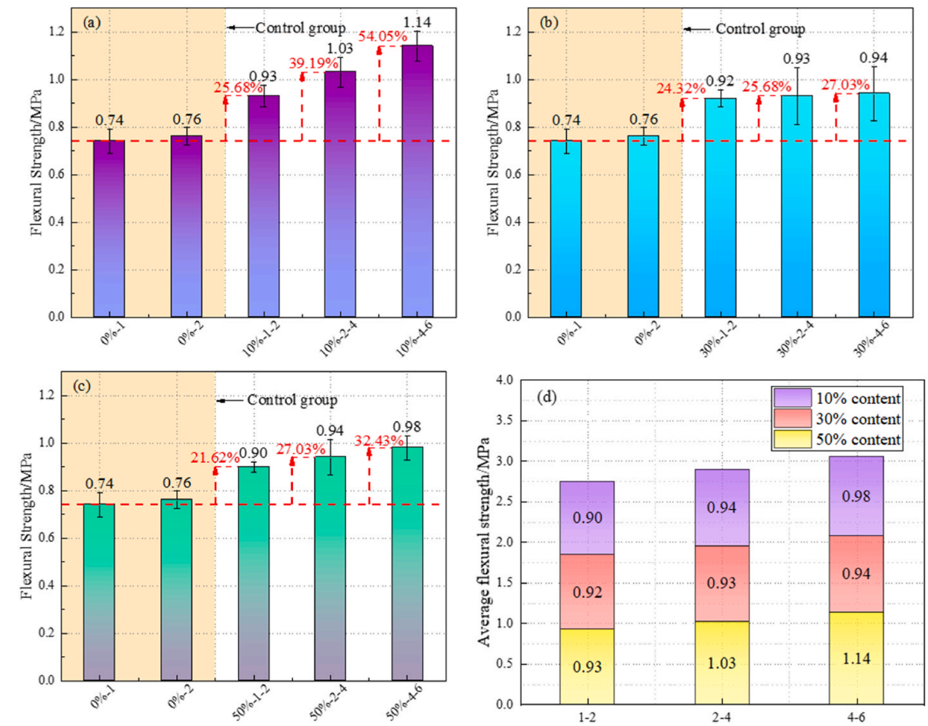

Fig. 8. Different gravel rock grain diameters on mean FS of FRCTRFs with a rate of (a) 10%; (b) 30%; (c) 50%; and (d) Stacking diagram under the influence of particle sizes.

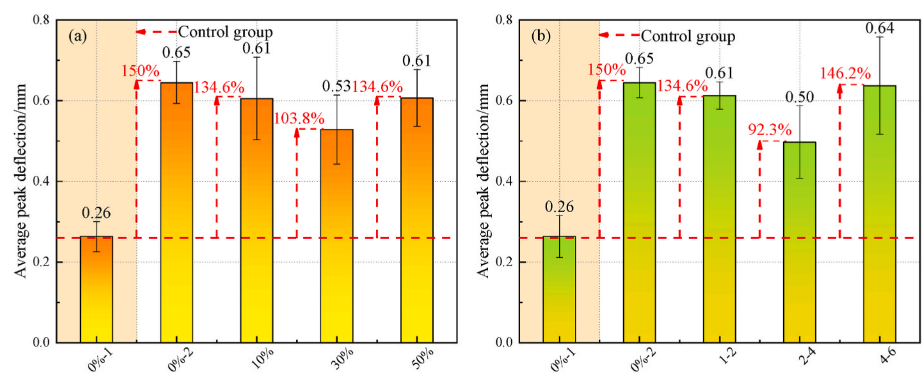

Fig. 9. The variation of peak deflection under the impact of dosage and grain size (a) content; and (b) grain size.

3.1.1. *Influence of gravel rock rate on FRCTRF's flexural strength*

Fig. 7 demonstrates gravel rock rate impact on mean flexural strength of FRCTRF specimens. It can be inferred that the use of partial gravel instead of partial tailings in the top layer or the addition of fiber in the bottom layer is useful for enhancing FRCTRFs' strength. Discrepancy characteristics of the strength evolution of FRCTRFs containing gravel are different under different gravel particle sizes. Fig. 7 (a–c) demonstrate that, mean FS value of the sample mixed with gravel is increased compared with the sample of 0%–1, with an increased range of 24.32%–54.05%. 10% - 1–2, 50% - 1–2, 30% - 1–2, 50% - 2–4, 30% - 2–4, 50% - 4–6 and 30% - 4–6 respectively increased by 25.68 %, 24.32 %, 21.62 %, 25.68 %, 27.03 %, 27.03 % and 32.43 %, The growth rate has changed relatively little. 10%-2-4 and 10%-1-2 increased by 39.19 % and 54.05 % respectively. Fig. 7(d) shows the stack bar chart of the average FS of each scheme under dosage's influence. By a dosage increase, mean FS displays a tendency of lessening initially and growing later. Overall, mechanical properties of FRCTRF specimens with 10 % gravel content are the best.

3.1.2. *Rock grain diameter effect on FRCTRF's stability behavior*

Fig. 8 reflects variation of average strength property of FRCTRF specimens considering particle size of gravel. Fig. 8(a–c) demonstrate that, it can be inferred that under the same gravel content, rising gravel grain diameter, mean flexural strength property shows a growing tendency. Fig. 8(d) illustrates that mechanical properties of FRCTRFs holding a particle size of 4–6 mm are the best, followed by those with a particle size of 2–4 mm.

3.2. *Deflection characteristics of FRCTRF specimens*

In this bending test, the addition of fiber changes FRCTRF's bending behavior. Peak rebound was used as a reference to analyze each group of specimens to scrutinize reinforcement fiber impact. The top rebound is the linear dislocation in specimen's axial track amid preliminary loading (with load of 50 N as starting value) and interval for which the highest strength is prolonged. Fig. 9 demonstrates variation law of peak deflection under the influence of mixing amount and particle size.

Fig. 9(a) and (b) demonstrates that, FRCTRF's peak deflection can be

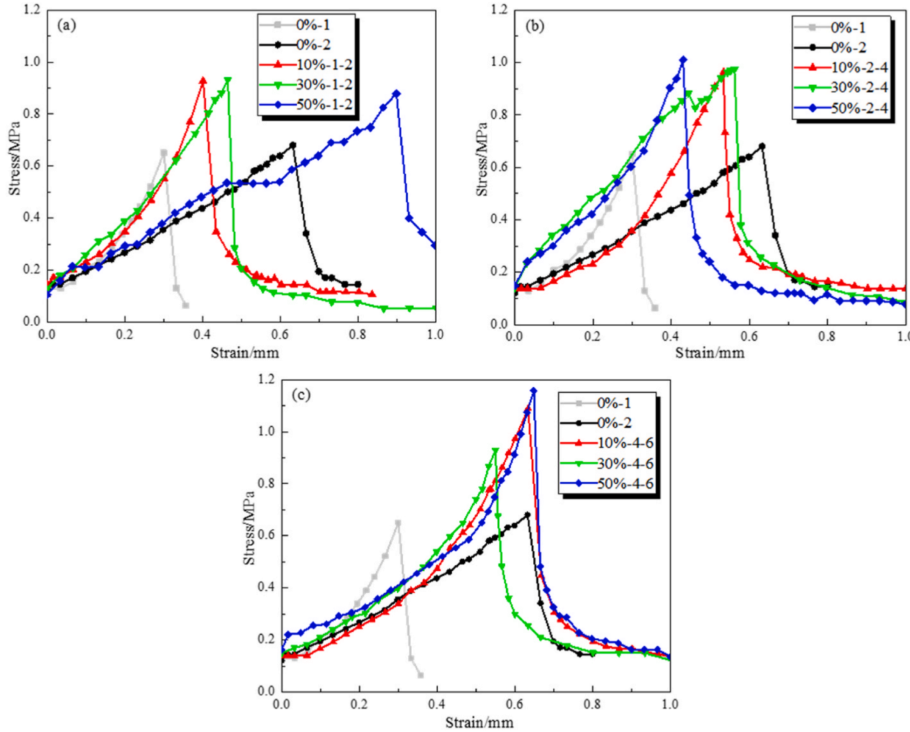

Fig. 10. Gravel rock rate impact on stress-strain correlation of FRCTRF holding a particle size of (a) 1–2 mm; (b) 2–4 mm; and (c) 4–6 mm.

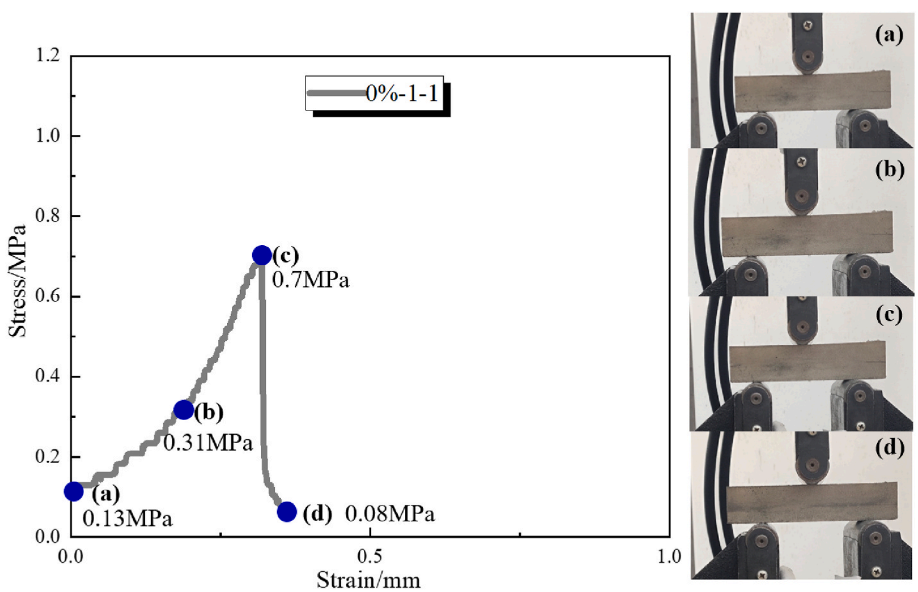

Fig. 11. 0%-1 specimen's failure mode.

greatly improved after PP fiber is added at the bottom, and the peak deflection of FRCTRF is increased by 150 % compared with the sample of 0%–2 (that is, the sample of only fiber added at the bottom) and 0%-1 (the vegan sample). The average peak deflection of FRCTRF with gravel added is less than 0%-2. With the inclusion of gravel, the peak deflection shows a certain variation law. By dosage's rise, peak deflection exhibited a tendency of decreasing initially and growing later. By gravel grain diameter's rise, peak deflection showed a tendency of diminishing initially and swelling later, but it had a larger increase than 0%-1. The larger peak deflection allows FRCTRF to withstand better deformation, so the addition of fiber or fiber and gravel can improve the mechanical properties of FRCTRF.

3.3. Gravel rock impact on fill's stress-strain relationship

Fig. 10 shows the variation law of FRCTRF's stress-strain curve. One can observe that FRCTRFs' strength decreases rapidly after reaching the peak value, in which 0%-1 samples have no posture ability following the top value, although other FRCTRF samples still have a confident posture ability following the top value. This is because PP fiber changes specimen's post-peak mechanical properties, which is in keeping with conclusions of preceding investigations. Fig. 10(a–c) demonstrates that, compared to sample 0%-2, FRCTRF sample containing gravel has a larger stress drop. Therefore, the addition of gravel makes FRCTRF sample more brittle after the peak.

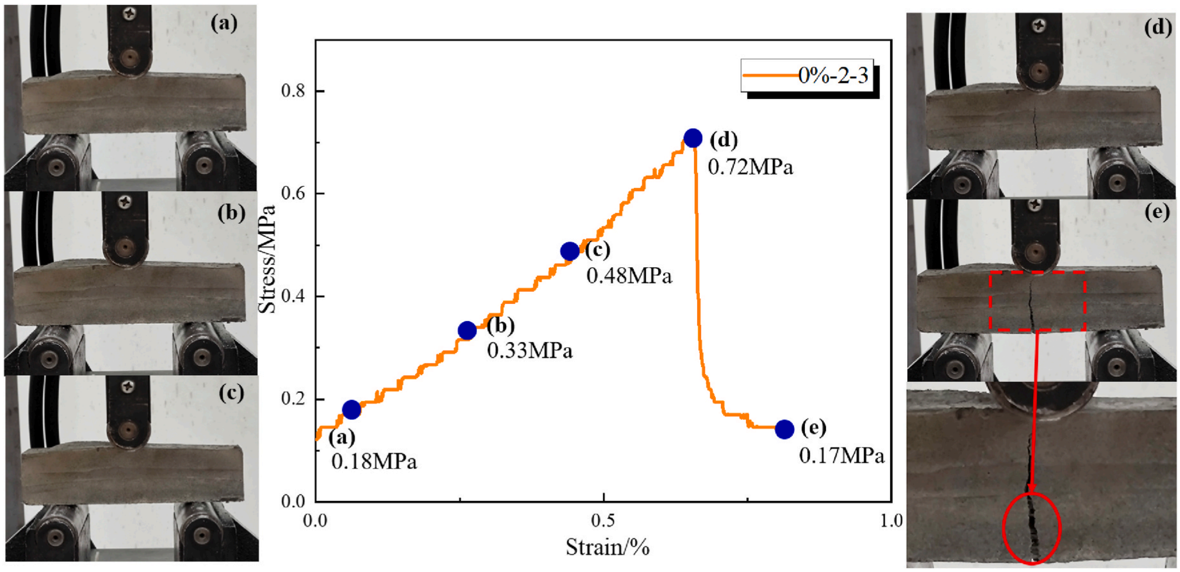

Fig. 12. 0%-2 specimen's failure mode.

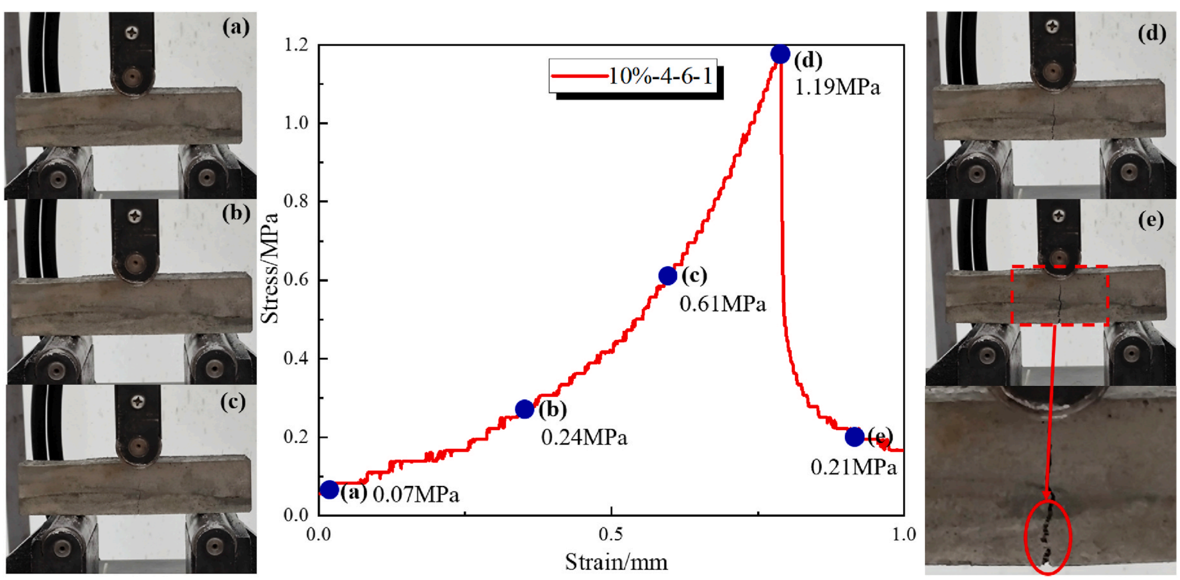

Fig. 13. 10%-4-6 specimen's failure mode.

3.4. Assessing FRCTRF's failure approaches

Fig. 11 demonstrates failure mode of sample 0%-1. One can witness that strength of sample 0%-1 drops rapidly after reaching the peak value, and no obvious cracks are found on surface.

Figs. 12 and 13 show the failure modes of samples 0%-2 and 10%-4-6. Microcracks appear on the surface of samples 0%-2 and 10%-4-6 in the early loading, and the microcracks gradually expand upward with the loading of samples. After reaching the peak, sample's bearing capacity decreases rapidly, and the cracks gradually open, at which time the PP fiber exposed to the air can be observed to play the role of bridge. Thus, it can be inferred that adding PP fiber can improve the post-peak mechanical properties of FRCTRF specimens.

3.5. Assessing FRCTRF's microstructural portrayal

Fig. 14 shows SEM images of five diverse FRCTRF rates: 0%-2, 10%-1-2, 10%-2-4, 10%-4-6, 30%-1-2, 50%-1-2. The pseudo-color image is processed by ImageJ software to improve the image resolution. Fig. 14 (a) and (b) show the microstructure of the control sample (0%-2). Obvious layers, pores, micro-cracks, large-size tailings particles, and PP fibers can be seen on the surface of sample. The width of the fibers is measured to be 140.8 μm, and large quantities of CSH and AFt on surface are its main products. Fig. 14(c) and (d) show 10%-1-2 specimen's microstructure. A micro-crack with a width of 39.3 μm is observed. At the same time, an obvious trace of broken stone with a size of 663.4 μm is observed. In Fig. 14(d), one can observe that CSH and AFt are its leading produces. Fig. 14(e) and (f) show the microstructure of 10%-2-4. Width of large pores is 414.8 μm and 452.4 μm, respectively. The width of two broken PP fibers is 190.8 μm, and there are also some tail sand particles with a size of 116.4 μm on the surface. C-S-H and AFt remain its main products. As shown in Fig. 14(g) and (h), a stratified interface and unbroken gravel particles with a size of 1869.4 μm can be observed inside 10%-4-6, and CSH and AFt on surface are its main products. As shown in Fig. 14(i), broken fibers and large numbers of big pores can be observed in interior of 30%-4-6, which may be the reason for its low

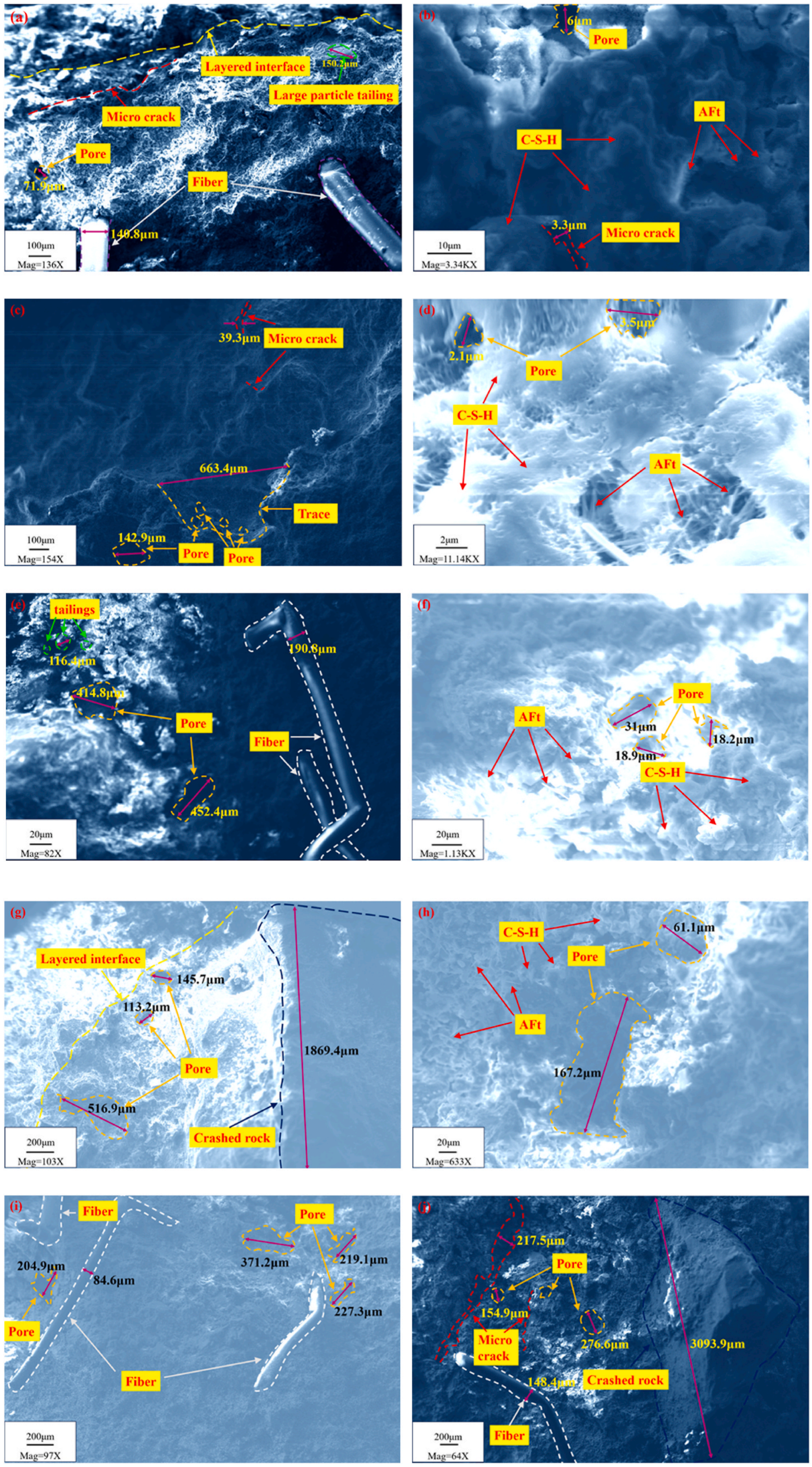

Fig. 14. SEM views of FRCTRF specimens: (a–b) 0%-2; (c–d) 10%-1-2; (e–f) 10%-2-4; (g–h) 10%-4-6; (i) 30%-1-2; and (j) 50%-1-2.

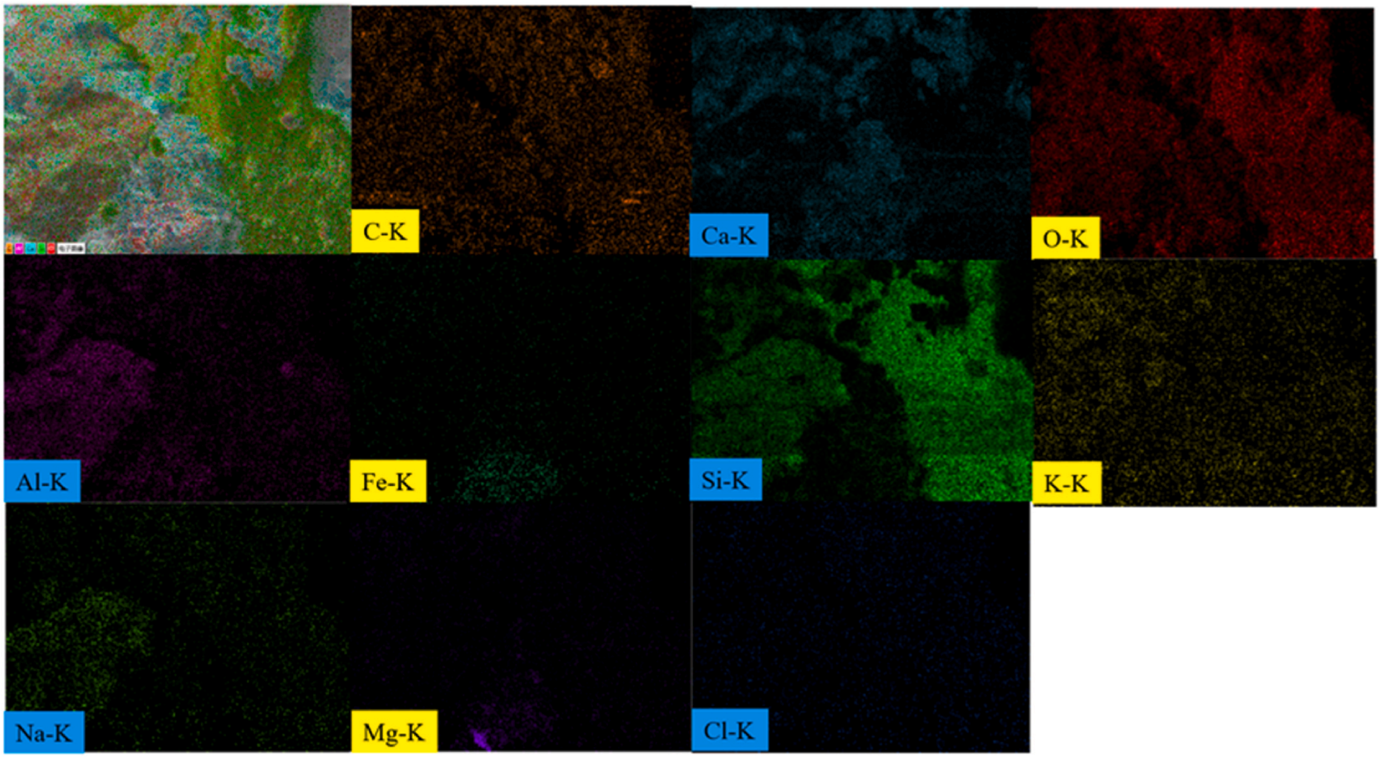

Fig. 15. FRCTRF's main element map based on SEM-EDS results.

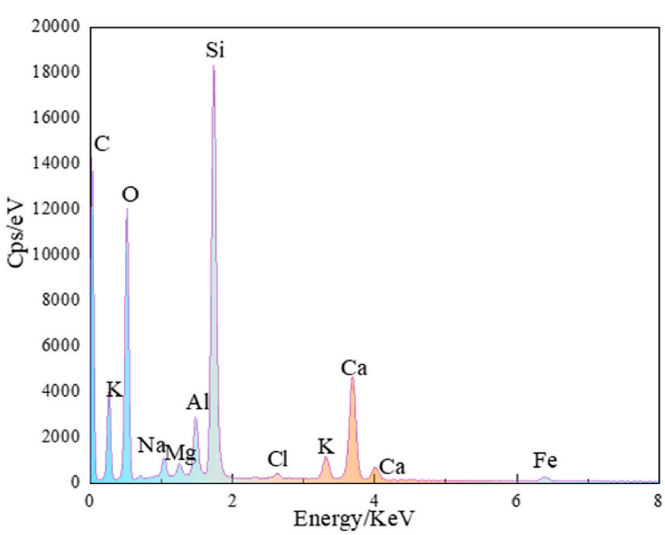

Fig. 16. EDS energy spectrum analysis diagram.

strength. Fig. 14(j) demonstrates that there are some micro cracks, pores, and large gravel particles in the microstructure of 50%-4-6, with a size of 3093.9 μm, and PP fibers on the surface with a width of 148.4 μm.

Figs. 15 and 16 demonstrate the sharing of basic essentials and SEM-EDS (examination of FRCTRF sample. Important elements existing in cementitious mine fill samples are C, Ca, O, Na, Si, Mg, Cl, K, Al, and Fe. C, O, Si, K, and Al values are the highest. They are clustered nearby CSH and improve FRCTRF's bending behavior.

4. Conclusions

Substituting mine waste with gravel rock as a backfill ingredient material was inspected in the current work. Various parameters (i.e., strength, damage and microstructure) of FRCTRF specimens considering diverse gravel rock rates and grain diameters were explored using three-point bending test and SEM-EDS. The resulting fundamental deductions were made from these lab-supported studies:

- o Adding fiber has a small impact on FRCTRF's flexural strength, while gravel rock has a major impact on its flexural strength. With difference in gravel particle size/content, the strength shows different changes, and the enhancement range is 21.62 %–54.05 %.
- o Adding fiber to the bottom of FRCTRF can enhance the peak deflection of FRCTRF, and the peak deflection of FRCTRF increases by 150% compared with the peak deflection of 0%–1 at 0%-2. Observing the peak deflection of FRCTRF with the addition of gravel, peak deflection of FRCTRF shows a tendency of decreasing initially and increasing by rising gravel particle size/rate.
- o Adding PP fiber mends FRCTRF's post-peak strength features. FRCTRFs containing gravel has a large stress drop. Thus, the addition of gravel makes FRCTRF more brittle after the peak.
- o The surface of FRCTRFs is observed to have pores, layered interfaces, broken fibers, broken stone traces, tailings particles, and broken stone particles, and the production is mainly CSH and AFt. Tiny pores could be witnessed at debris-shedding marks, suggesting that the presence of debris caused FRCTRF to create more pores.

In summary, this study has experimentally demonstrated that FRCTRF offers much superior strength properties and can be used as an effective reinforcement tool in filling construction. However, field-scale experimental studies are needed, especially *in situ* fill tests, to clearly reveal the behavior of fill and the problems that may be encountered in practice. In particular, the strength of fills reinforced with fiber reinforcement and fills supported by different chemical additives will be discussed in depth by the same authors in the next studies.

CRediT authorship contribution statement

Hao Qin: Writing – original draft, Methodology, Investigation, Conceptualization. **Shuai Cao:** Writing – review & editing, Supervision, Methodology, Funding acquisition. **Erol Yilmaz:** Writing – review & editing, Visualization, Supervision, Methodology.

Declaration of competing interest

The authors declare that they have no known competing financial interests or personal relationships that could have appeared to influence the work reported in this paper.

Acknowledgments

The present investigation is generously secured by China's National Key R@D Program under grant number 2022YFC2905004. We acknowledge the support of time and facilities from USTB.

Data availability

No data was used for the research described in the article.

References

Ahmad, W., Khan, M., Smarzewski, P., 2021. Effect of short fiber reinforcements on fracture performance of cement-based materials: a systematic review approach. Materials 14, 1745.

Ajouguim, S., Page, J., Djelal, C., Saâdi, L., 2023. Effect of treated Alfa fibers on hydration kinetics, mechanical, and adhesion properties of fiber cement composite. J. Build. Eng. 71, 106558.

Benzaazoua, M., Belem, T., Yilmaz, E., 2006. Novel lab tool for paste backfill. Can. Min. J. 127 (3), 31–32.

Bianchi, I., Volpe, S., Fiorito, F., Forcellese, A., Sangiorgio, V., 2024. Life cycle assessment of building envelopes manufactured through different 3D printing technologies. J. Clean. Prod. 440, 140905.

Bull, A.J., Fall, M., 2020. Thermally induced changes in metalloid leachability of cemented paste backfill that contains blast furnace slag. Miner. Eng. 156, 106520.

Carnogursky, E.A., Fall, M., Haruna, S., 2023. Rheology and setting time of saline cemented paste backfill. Miner. Eng. 202, 108258.

Chen, X., Shi, X., Zhou, J., Yu, Z., Huang, P., 2020. Determination of mechanical, flowability, and microstructural properties of cemented tailings backfill containing rice straw. Construct. Build. Mater. 246, 118520.

Chompoorat, T., Likitlersuang, S., Buathong, P., Jongpradist, P., Jamsawang, P., 2023. Flexural performance and microstructural characterization of cement-treated sand reinforced with palm fiber. J. Mater. Res. Technol. 25, 1570–1584.

Consoli, N.C., Nierwinski, H.P., da Silva, A.P., Sosnoski, J., 2017. Durability and strength of fiber-reinforced compacted gold tailings-cement blends. Geotext. Geomembranes 45 (2), 98–102.

Dash, B., Giri, J.P., Raju, P.M., Dora, D.T.K., 2023. Simultaneous influence of processed cellulose acetate fiber reinforcement and recycled aggregate replacement on mechanical and durability performances of concrete. Construct. Build. Mater. 401, 132950.

de Moraes, M.J.B., Nagata, E.Y., Duran, A.J.F.P., Rossignolo, J.A., 2024. Alkali activated materials applied in 3D printing construction: a review. Heliyon 10 (5), e26696.

Dong, P., Ding, W., Yuan, H., Wang, Q., 2022. 3D-printed polymeric lattice-enhanced sustainable municipal solid waste incineration fly ash alkali-activated cementitious composites. Dev. Built Environ. 12, 100101.

Falliano, D., Parmigiani, S., Suarez-Riera, D., 2022. Stability, flexural behavior and compressive strength of ultra-lightweight fiber-reinforced foamed concrete with dry density lower than 100 kg/m3. J. Build. Eng. 51, 104329.

Fang, K., Zhang, J., Cui, L., Haruna, S., Li, M., 2023. Cost optimization of cemented paste backfill: state-of-the-art review and future perspectives. Miner. Eng. 204, 108414.

Gao, R.G., Wang, W.J., Xiong, X., Li, J.J., Xu, C., 2023. Effect of curing temperature on the mechanical properties and pore structure of cemented backfill materials with waste rock-tailings. Construct. Build. Mater. 409, 133850.

Gencel, O., Nodehi, M., Bayraktar, O.Y., Kaplan, G., Benli, A., Gholampour, A., Ozbakkaloglu, T., 2022. Basalt fiber-reinforced foam concrete containing silica fume: an experimental study. Construct. Build. Mater. 326, 126861.

Guler, S., Akbulut, Z.F., 2023. The effects of single and hybrid polypropylene fibers on the workability and residual strength properties of concrete road pavements against freeze-thaw cycles. Arabian J. Sci. Eng. 48, 13489–13505.

Haruna, S., Fall, M., 2022. Reactivity of cemented paste backfill containing polycarboxylate-based superplasticizer. Miner. Eng. 188, 107856.

Hou, Y., Yin, S., Chen, X., Zhang, M.Z., Du, H.H., 2023. Experimental study on time-dependent rheological properties and mechanical performance of cemented fine tailings backfill mixed with polypropylene fiber. Environ. Sci. Pollut. Control Ser. 30, 102862–102879.

Hou, Y., Yang, K., Yin, S., Yu, X., Kou, P., Wang, Y., 2024. Enhancing workability, strength, and microstructure of cemented tailings backfill through mineral admixtures and fibers. J. Build. Eng. 84, 108590.

Hu, L., Chen, Z., Yang, H., Zhu, X., Wang, W., 2024. Mechanical properties and microstructure evolution of phosphate slag-cement based materials under varied curing temperatures. Dev. Built Environ. 18, 100389.

Huang, Z., Cao, S., Yilmaz, E., 2021. Investigation on the flexural strength, failure pattern and microstructural characteristics of combined fibers reinforced cemented tailings backfill. Construct. Build. Mater. 300, 124005.

Huang, Z., Cao, S., Yilmaz, E., 2023. Microstructure and mechanical behavior of cemented gold/tungsten mine tailings-crushed rock backfill: effects of rock gradation and content. J. Environ. Manag. 339, 117897.

Jan, A., Pu, Z., Khan, K.A., Ahmad, I., Khan, I., 2022. Effect of glass fibers on the mechanical behavior as well as energy absorption capacity and toughness indices of concrete bridge decks. Silicon 14, 2283–2297.

Jiang, H.Q., Fall, M., Cui, L., 2017. Freezing behaviour of cemented paste backfill material in column experiments. Construct. Build. Mater. 147, 837–846.

Jiang, P., Chen, L., Li, N., Qian, J., Wang, W., 2022. Study on the mechanical properties of fiber-modified iron tailings stabilized by lime and fly ash based on energy analysis. Case Stud. Constr. Mater. 17, e01638.

Jiang, M., Cao, S., Yilmaz, E., 2024a. Exploring microstructure and mechanical features of coupled cementitious tail-sand concrete by partial replacement of tungsten tailings. Proc. Safet. Environ. Prot., In-Press. https://doi.org/10.1016/j.psep.2024.08.100.

Jiang, T., Cao, S., Yilmaz, E., 2024b. Microstructure evolution and mechanical behavior of foamed cement-based tail backfills under varying fiber types and concentrations. Environ. Sci. Pollut. Control Ser. 31, 52181–52197.

Jiao, H., Zhang, Q., Yang, Y., Yang, T., 2023. Effect of interface roughness on mechanical properties of layered cemented tailings backfill. Construct. Build. Mater. 409, 134071.

Jo, B.-W., Chakraborty, S., Lee, Y.S., 2015. Hydration study of the polymer modified jute fibre reinforced cement paste using analytical techniques. Construct. Build. Mater. 101 (1), 166–173.

Johansson, L., Bahrami, A., Wallhagen, M., Cehlin, M., 2024. A comprehensive review on properties of tailings-based low-carbon concrete: mechanical, environmental, and toxicological performances. Dev. Built Environ. 18, 100428.

Kasap, T., Yilmaz, E., Sari, M., 2022. Effects of mineral additives and age on microstructure evolution and durability properties of sand-reinforced cementitious mine backfills. Construct. Build. Mater. 352, 129079.

Komurlu, E., 2023. Use of microgrid fibre as a new reinforcement additive to improve compressive and tensile strength values of cemented rock fill mixes. Int. J. Min. Reclamat. Environ. 37 (10), 760–768.

Koohestani, B., Darban, A.K., Darezerehshki, E., Mokhtari, P., Yilmaz, E., Yilmaz, E., 2018. The influence of sodium and sulfate ions on total solidification and encapsulation potential of iron-rich acid mine drainage in silica gel. J. Environ. Chem. Eng. 6 (2), 3520–3527.

Li, J.J., Cao, S., Yilmaz, E., 2021. Characterization of macro mechanical properties and microstructures of cement-based composites prepared from fly ash, gypsum and steel slag. Minerals 12 (1), 6.

Li, J.J., Cao, S., Song, W.D., 2023a. Flexural behavior of cementitious backfill composites reinforced by various 3D printed polymeric lattices. Compos. Struct. 323, 117489.

Li, J.J., Cao, S., Song, W.D., 2023b. Distribution development of pore/crack expansion and particle structure of cemented solid-waste composites based on CT and 3D reconstruction techniques. Construct. Build. Mater. 376, 130966.

Li, Z., Sun, W., Gao, T., Zhao, J., Lu, K., Cheng, H., 2023c. Experimental study on evolution of pore structure of inclined layered cemented tailings backfill based on X-ray CT. Construct. Build. Mater. 366, 130242.

Lyu, H., Chen, Y., Pu, H., Ju, F., Zhang, K., Li, Q., Wu, P., 2023. Dynamic properties and fragmentation mechanism of cemented tailings backfill with various particle size distributions of aggregates. Construct. Build. Mater. 366, 130084.

Naoum, M.C., Papadopoulos, N.A., Voutetaki, M.E., Chalioris, C.E., 2023. Structural health monitoring of fiber-reinforced concrete prisms with polyolefin macro-fibers using a piezoelectric materials network under various load-induced stress. Buildings 13, 2465.

Niu, H., Abdulkareem, M., Sreenivasan, H., Kantola, A.M., Havukainen, J., Horttanainen, M., Telkki, V.-V., Kinnunen, P., Illikainen, M., 2020. Recycling mica and carbonate-rich mine tailings in alkali-activated composites: a synergy with metakaolin. Miner. Eng. 157, 106535.

Perumal, P., Niu, H., Kiventerä, J., Kinnunen, P., Illikainen, M., 2020. Upcycling of mechanically treated silicate mine tailings as alkali activated binders. Miner. Eng. 158, 106587.

Qi, C.C., Fourie, A., 2019. Cemented paste backfill for mineral tailings management: review and future perspectives. Miner. Eng. 144, 106025.

Qin, S., Cao, S., Yilmaz, E., Li, J.J., 2021. Influence of types and shapes of 3D printed polymeric lattice on ductility performance of cementitious backfill composites. Construct. Build. Mater. 307, 124973.

Qin, H., Cao, S., Yilmaz, E., 2024. Mechanical, energy evolution, damage and microstructural behavior of cemented tailings-rock fill considering rock content and size effects. Construct. Build. Mater. 411, 134449.

Qiu, H., Zhang, F., Liu, L., Huan, C., Hou, D., Kang, W., 2022. Experimental study on acoustic emission characteristics of cemented rock-tailings backfill. Construct. Build. Mater. 315, 125278.

Qiu, Y., Wang, Y., Liu, Y., Zhang, L., Chen, Y., Li, C., Wu, T., Wang, C., 2023. Development of fiber compound foaming agent and experimental study on application performance of foamed lightweight soil. Appl. Rheol. 33 (1), 20230108.

Sadrossadat, E., Basarir, H., Luo, G., Karrech, A., Durham, R., Fourie, A., Elchalakani, M., 2020. Multi-objective mixture design of cemented paste backfill using particle swarm optimisation algorithm. Miner. Eng. 153, 106385.
Samiratou Yaya, N., Cao, S., Yilmaz, E., 2024. Effect of 3D printed skeleton shapes on strength behavior, stress evolution and microstructural response of cement-based tailings backfills. Construct. Build. Mater. 432, 136699.
Sari, M., Yilmaz, E., Kasap, T., 2023. Long-term ageing characteristics of cemented paste backfill: usability of sand as a partial substitute of hazardous tailings. J. Clean. Prod. 401, 136723.
Sun, W., Gao, T., Zhao, J., Cheng, H., 2023. Research on fracture behavior and reinforcement mechanism of fiber-reinforced locally layered backfill: experiments and models. Construct. Build. Mater. 366, 130186.
Wang, Y., Yu, Z., Wang, H., 2021a. Experimental investigation on some performance of rubber fiber modified cemented paste backfill. Construct. Build. Mater. 271, 121586.
Wang, J., Fu, J.X., Song, W.D., Zhang, Y.F., Wu, S., 2021b. Acoustic emission characteristics and damage evolution process of layered cemented tailings backfill under uniaxial compression. Construct. Build. Mater. 295, 123663.
Wang, S., Mo, D., Wu, Q., Bu, X., Xue, J., Zhang, C., 2023a. Design and analysis of sustainable models for Qinling ecological protection and mining development. Miner. Eng. 204, 108446.
Wang, C., Liao, F., Wang, G., Qu, S., Mao, H., Bai, Y., 2023b. Hydrogeochemical evolution induced by long-term mining activities in a multi-aquifer system in the mining area. Sci. Total Environ. 854, 158806.
Wang, J., Yu, Q., Xiang, Z., Fu, J., Wang, L., Song, W.D., 2023c. Influence of basalt fiber on pore structure, mechanical performance and damage evolution of cemented tailings backfill. J. Mater. Res. Technol. 27, 5227–5242.
Wang, B.W., Kang, M.C., Liu, C.Y., Yang, L., Li, Q.L., Zhou, S.L., 2024. Experimental study on mechanical and microstructure properties of cemented tailings-waste rock backfill with continuous gradation. J. Build. Eng. 95, 110146.
Xu, W.B., Li, Q.L., Zhang, Y., 2019. Influence of temperature on compressive strength, microstructure properties and failure pattern of fiber-reinforced cemented tailings backfill. Construct. Build. Mater. 222, 776–785.
Xu, W.B., Tian, M.M., Li, Q.L., 2020. Time-dependent rheological properties and mechanical performance of fresh cemented tailings backfill containing flocculants. Miner. Eng. 145, 106064.
Xu, X., An, N., Fang, K., 2022. Experimental investigation into the temperature effect on the shear behavior of the fiber-reinforced interface between rock and cemented paste backfill. Construct. Build. Mater. 356, 129280.
Xue, G.L., Yilmaz, E., Feng, G.R., Cao, S., 2021. Bending behavior and failure mode of cemented tailings backfill composites incorporating different fibers for sustainable construction. Construct. Build. Mater. 289, 123163.
Xue, G.L., Yilmaz, E., Feng, G.R., Cao, S., 2022. Analysis of tensile mechanical characteristics of fiber reinforced backfill through splitting tensile and three-point bending tests. Int. J. Min. Reclamat. Environ. 36 (3), 218–234.
Xue, G.L., Yilmaz, E., Wang, Y.D., 2023. Progress and prospects of mining with backfill in metal mines in China. Int. J. Miner. Metall. Mater. 30 (8), 1455–1473.
Yan, B.X., Jia, H.W., Yilmaz, E., Lai, X.P., Shan, P.F., Hou, C., 2022. Numerical study on microscale and macroscale strength behaviors of hardening cemented paste backfill. Construct. Build. Mater. 321, 126327.
Yang, L., Li, J., Liu, H., Jiao, H., Yin, S., Chen, X., Yu, Y., 2023. Systematic review of mixing technology for recycling waste tailings as cemented paste backfill in mines in China. Int. J. Miner. Metall. Mater. 30, 1430–1443.
Yang, G., Liu, F., Xie, Q., Yang, M., Li, Y., Kumar, E.R., Sun, J., 2024. Exploration of iron ore tailings with high volume in sustainable cement and ecofriendly cementitious material. Dev. Built Environ. 19, 100482.
Yilmaz, E., Belem, T., Benzaazoua, M., Bussiere, B., 2010. Assessment of the modified CUAPS apparatus to estimate *in situ* properties of cemented paste backfill. Geotech. Test J. 33 (5), 351–362.
Yilmaz, E., Belem, T., Benzaazoua, M., 2013. Study of physico-chemical and mechanical characteristics of consolidated and unconsolidated cemented paste backfills. Miner. Resourc. Manag. 29 (1), 81–100.
Yin, S.H., Yan, Z.P., Chen, X., Yan, R.F., Chen, D.P., Chen, J.W., 2023. Mechanical properties of cemented tailings and waste-rock backfill (CTWB) materials: laboratory tests and deep learning modeling. Construct. Build. Mater. 369, 130610.
Yu, Z., Qin, N., Huang, S., Li, J., Wang, Y., 2022. Performance characteristics of cemented tailings containing crumb rubber as a filling material. Adv. Mater. Sci. Eng. 2022, 3117806.
Zhang, H., Cao, S., Yilmaz, E., 2022. Influence of 3D-printed polymer structures on dynamic splitting and crack propagation behavior of cementitious tailings backfill. Construct. Build. Mater. 343, 128137.
Zhang, H., Cao, S., Yilmaz, E., 2023. Carbon nanotube reinforced cementitious tailings composites: links to mechanical and microstructural characteristics. Construct. Build. Mater. 365, 130123.
Zhang, X., Xue, X., Ding, D., Sun, P., Li, J., He, Y., 2024. A study of the mechanical properties, environmental effect, and microscopic mechanism of phosphorus slag-based uranium tailings backfilling materials. J. Clean. Prod. 446, 141306.
Zhao, Z., Cao, S., Yilmaz, E., 2023a. Effect of layer thickness on the flexural property and microstructure of 3D-printed rhomboid polymer-reinforced cemented tailing composites. Int. J. Miner. Metall. Mater. 30 (2), 236–249.
Zhao, Y., Zhao, G., Xu, L., Zhou, J., Huang, X., 2023b. Mechanical property evolution model of cemented tailings-rock backfill considering strengthening and weakening effects. Construct. Build. Mater. 377, 131081.
Zhu, D., Zhang, S., Wu, X., 2024a. Study on the flexural performance and microstructure of lithium feldspar tailings cementitious filler using mixed fibers. Dev. Built Environ. 18, 100455.
Zhu, D., Huang, N., Li, W., Li, J., Wu, X., 2024b. Effect of different fibers and fiber contents on the mechanical properties and failure behavior of early age cemented lithium feldspar tailings backfill. Dev. Built Environ. 19, 100495.
Zou, S., Guo, W., Wang, S., Gao, Y., Qian, L., Zhou, Y., 2023. Investigation of the dynamic mechanical properties and damage mechanisms of fiber-reinforced cemented tailing backfill under triaxial split-Hopkinson pressure bar testing. J. Mater. Res. Technol. 27, 105–121.
Zou, S.X., Cao, S., Yilmaz, E., 2024. Enhancing flexural property and mesoscopic mechanism of cementitious tailings backfill fabricated with 3D-printed polymers. Construct. Build. Mater. 414, 135009.